Extended asymmetric hot region formation due to shockwave interactions following void collapse in shocked high explosive

Tzu-Ray Shan, Ryan R. Wixom, and Aidan P. Thompson

Phys. Rev. B **94**, 054308 — Published 11 August 2016

DOI: 10.1103/PhysRevB.94.054308

Extended Asymmetric Hot Region Formation due to Shockwave Interactions Following Void Collapse in Shocked High Explosive

Tzu-Ray Shan,* Ryan R. Wixom, and Aidan P. Thompson

Sandia National Laboratories, Albuquerque, New Mexico 87185

(Dated: July 27, 2016)

Abstract

In both continuum hydrodynamics simulations and also multi-million atom reactive molecular dynamics simulations of shockwave propagation in single crystal pentaerythritol tetranitrate (PETN) containing a cylindrical void, we observed the formation of an initial radially symmetric hot spot. By extending the simulation time to the nano-second scale, however, we observed the transformation of the small symmetric hot spot into a *longitudinally asymmetric hot region* extending over a much larger volume. Performing reactive molecular dynamics shock simulations using the reactive force field (ReaxFF) as implemented in the LAMMPS molecular dynamics package, we showed that the longitudinally asymmetric hot region was formed by coalescence of the primary radially symmetric hot spot with a secondary triangular hot zone. We showed that the triangular hot zone coincided with a double-shocked region where the primary planar shockwave was overtaken by a secondary cylindrical shockwave. The secondary cylindrical shockwave originated in void collapse after the primary planar shockwave had passed over the void. A similar phenomenon was observed in continuum hydrodynamics shock simulations using the CTH hydrodynamics package. The formation and growth of extended asymmetric hot regions on nano-second timescales has important implications for shock initiation thresholds in energetic materials.

I. INTRODUCTION

Material defects and heterogeneities in energetic materials play a key role in the onset of shock-induced chemical reactions and the ignition of hotspots by lowering initiation thresholds.[1–5] Defects and heterogeneities concentrate shockwave energy in small regions, resulting in local excitation of the material. This allows exothermic chemical reactions to occur, leading to further energy release, chemical reaction initiation, and detonation. These defects and heterogeneities include dislocation[6,7], shear band[8,9], grain boundary[10,11], entrained solvent[12], and porosity/cavity/void[13–18]. We have previously investigated void collapse behavior and void collapse induced hot spot growth in pentaerythritol tetranitrate (PETN) containing a void 20 nm in diameter using large-scale reactive molecular dynamics (MD) simulations.[19] We compared a 3-dimensional spherical void and a 2-dimensional cylindrical void. It was shown that although both overall temperature and hot spot temperature are lower in the cylindrical void configuration, phenomena leading to hot spot formation including jetting of upstream void fragments, void collapse, and collision between upstream void fragments and downstream void surface are qualitatively equivalent to those occurring in the spherical void configuration.[19] It is therefore reasonable to investigate hot spot formation and growth using the cylindrical void configuration, with the main advantage being a great reduction of the thickness of the simulations in one lateral direction, leading to a commensurate increase in computational efficiency. In this work, therefore, we investigated shock-induced void collapse and hot spot growth behavior around a 20 nm (in diameter) cylindrical void, with the simulation time extending to half a nanosecond after initial impact.

II. SIMULATION DETAILS

We used the ReaxFF reactive force field as implemented in Large-scale Atomic/Molecular Massively Parallel Simulator (LAMMPS) molecular dynamics package[20,21]. ReaxFF is an advanced bond-order variable charge force field that enables large-scale simulations of chemically reactive systems. Full details of ReaxFF can be found elsewhere.[22–24] The ReaxFF force field description for PETN used in this work was developed for nitramines[25] and was extended to triacetone triperoxide (TATP)[26] and nitromethane[27], and it has been previously applied in several shock simulation studies of PETN[19,28–30]. We have shown that this force

field description accurately reproduces PETN gas phase dissociation barriers along several different reaction channels, reasonably predicts shock properties of PETN crystals including U_S-U_P Hugoniot states and shock initiation stress along different orientations, and explains orientation-dependent sensitivity of PETN crystals.[30]

In this work, we prepared a PETN crystal containing a cylindrical void (containing only vacuum) that is 20 nm in diameter. The simulation box had dimensions of 302 nm × 221 nm × 1.4 nm. The [110], [$\bar{1}$10], and [001] crystallographic orientations were aligned with the x, y, and z directions of the simulation box, respectively. Periodic boundary conditions were applied in the transverse y and z directions, while the x direction was non-periodic, resulting in {110} free surfaces at the left and right ends of the crystal. A reflective boundary was applied at the left end of the cell, which mimicked an infinite impedance flyer plate. The void was created by removing PETN molecules whose centers of mass lay in a cylindrical region of 20 nm diameter, with the cylindrical axis oriented along the z axis and passing through a point with x coordinate 120 nm from the left free surface and y coordinate midway between the upper and lower periodic boundaries.

The PETN crystal was first equilibrated at 300 K and zero pressure with a density of 1.67 g/cm^3. After equilibration, all the atoms in the PETN crystal were assigned an additional particle/impact velocity (U_P) in the negative x direction, colliding it against the reflective boundary. The equations of motion of the atoms were integrated using the velocity Verlet discretization with a timestep of 0.1 fs. For full details of the molecular dynamics methodology, see[30].

III. RESULTS AND DISCUSSIONS

A. Hot spot formation and growth

The impact velocity assigned to the PETN crystal was 1.25 km/s. When the PETN crystal impacted against the stationary wall, a supported planar shockwave with a shock-wave velocity of 4.64 km/s propagated through the crystal from left to right along the [110] crystallographic orientation yielding shock-induced compression of the crystal. The shock-wave reached the free surface on the right side after 64.6 ps, and the backward rarefaction wave that would normally form was suppressed using the shock front absorbing boundary

condition (ABC) method[31], allowing us to continue the simulation from 64.6 to 500.0 ps. Temperature maps from the molecular dynamics simulation at intervals of 0.1 ns are shown in Figure 1. Temperature was calculated by grouping atoms into small cubic regions based on their positions, and the temperature of each region was calculated as the average kinetic energy of each atomic degree of freedom after subtracting the mass-weighted streaming velocity of all the atoms in the region. After the cylindrical void fully collapsed 29 ps after the initial impact, a small hot spot that was roughly the area of the original void area formed. The hot spot size grew slowly for the first 0.2 ns, but then the growth rate increased strongly from 0.2 to 0.4 ns while the intensity of the hot spot core also increased and the shape of the hot spot remained radially symmetric. Between 0.4 and 0.5 ns, the hot spot size grew very rapidly to fill most of the simulation cell, resulting in an extended hot region with a longitudinally asymmetric morphology (Figure 1f).

Plotted in Figure 2a is hot spot size and growth rate as a function of simulation time, with hot spot size being defined by summing the area of the regions with temperature greater than 600 K and the growth rate being estimated from the change in hot spot size between consecutive snapshots taken at 10 ps intervals. As shown in Figure 2a, both hot spot size and growth rate increased steadily from 0.2 to 0.45 ns, and the shapes of the two curves are similar, indicating an exponential relationship between the two. In the final 0.5 ns of the simulation, the growth rate accelerates far beyond that expected from exponential growth, as the secondary hot zone starts to rapidly add to the total hot spot area (see below).

The populations of select molecular species are plotted in Figure 2b, making use of the on-the-fly molecular species analysis capability in LAMMPS. For the first 0.2 ns, only the reactant PETN, intermediate NO_2, and very small amount of product H_2O existed in the system. From 0.2 to 0.4 ns, the rate of chemical reactions started to accelerate: PETN disappeared more rapidly, accompanied by rapid increases in NO_2 and product species including H_2O, CO_2, and N_2. Exothermic chemical reactions, which are those producing stable low-energy product species, became dominant from 0.4 ns onward, releasing even more energy into the system. Comparing Figures 2a and 2b, a strong temporal coupling between hot spot growth and chemical reaction can be inferred.

B. Formation of the asymmetric hot spot and secondary hot zone

Examining Figure 1 we also observed an asymmetric growth of the hot spot at later times (most obvious in Figure 1f). A radially symmetric hot spot that was approximately 46 nm in diameter at 0.3 ns evolved into a distorted diamond shape at 0.5 ns with dimensions of 110 nm and 90 nm in the longitudinal and transverse directions, respectively. Illustrated in Figure 3 are temperature maps at 0.1 ns and 0.375 ns after initial impact, both far behind the planar shockwave. In order to render the secondary hot zone more discernible, the color map only distinguishes temperatures in the range 400 to 800 K. At 0.1 ns, the primary hot spot is the center red region, and ahead of the primary hot spot we can see a faint triangular region - shown in blue - with an averaged temperature of 480 K, with a colder shadow separating it from the primary hot spot. Since this triangular region is higher in temperature compared to surrounding compressed material while much lower in temperature compared to the primary hot spot, we refer to it as a *secondary hot zone*. At 0.375 ns (illustrated in Figure 3b), in addition to the growth of the primary hot spot, the secondary hot zone also became slightly larger and hotter. The contrast with the cooler surrounding material has become more pronounced. Illustrated in Figure 4 is the spatial distribution of unreacted PETN, with each sphere representing a PETN molecule. Regions that correspond to the primary hot spot and the secondary hot zone have significantly fewer unreacted PETN molecules, indicating a strong spatial coupling between hot spot formation/growth and chemical reaction. Regions inside the secondary hot zone not only have elevated temperature but also enhanced chemical reactivity. The shape of the primary hot spot became increasingly asymmetric from 0.375 ns onward, as a result of the interaction between the primary hot spot and the secondary hot zone.

C. Secondary shockwave

In this section we show that the formation of the secondary hot zone is caused by the secondary shockwave that is generated upon void collapse. Figure 5 illustrates a sequence of density maps from 25 to 50 ps after initial impact: uncompressed material ahead of the planar shockwave has a density of 1.67 g/cc (shown in blue), while compressed material behind the shockwave is shown in yellow, orange, or red, depending on density values. At

25 ps the primary, planar shockwave passed over the void, ejecting a jet of material from the upstream void surface into the void. At 29 ps collision between the jet and the downstream void surface occurred, resulting in void collapsed. At the same time, pinning of the shockwave[16] around the void was also observed. The planar shockwave unpinned from the collapsed void at 32 ps, accompanied by the formation of a cylindrical secondary shockwave originating from the center of the collapsed void. From 35 to 46 ps we can see both the primary planar shockwave and the secondary cylindrical shock advance: the planar shockwave advancing downstream along $+x$ and the cylindrical shockwave advancing radially outward. The secondary cylindrical shockwave has a shockwave velocity of 6.40 km/s, faster than the primary planar shockwave (4.64 km/s). As a result the cylindrical shockwave progressively overtakes a wider and wider segment of the planar shockwave. The contact length between the two shockwaves increased from approximately 15 nm at 35 ps to approximately 110 nm at 46 ps.

Plotted in Figure 6 is a time sequence of density profiles (relative to uncompressed PETN) at positions located just behind the planar shock front. Since the shockwave near the void is locally non-planar, as shown in Figures 5a and 5b, we take that into account when selecting which cubic region to use, always picking the one just behind the local position of the shock front. The profiles are plotted with respect to the y coordinate. At 25 ps only the primary planar shockwave was present, and as a result the density is everywhere approximately 0.45 g/cc larger than the uncompressed PETN. The planar shock front density near the void (100 to 120 nm along $[\bar{1}10]$) was slightly lower, due to the early rarefaction wave coming back from the void surface. At 29 ps, after the void has collapsed, the secondary cylindrical shockwave has caught up with the primary planar shockwave, creating a *double-shocked* region and raising the density increase to approximately 0.8 g/cc, which is 0.4 g/cc larger than planar shock front. From 32 to 46 ps the double-shocked region continued to grow in width due to the advancing secondary circular shockwave, but the strength of the double-shocked region gradually decreased. After 50 ps, the double-shocked region is barely discernible. The area swept through by the double-shocked region after 50 ps coincides precisely with the triangular secondary hot zone that forms much later (Figure 3). This demonstrates that the extended asymmetric hot region is a direct result of the local reinforcement of the shockwave energy caused by the interaction between the primary planar shockwave and the secondary circular shockwave.

D. Comparison to hydrodynamic simulation

Analogous to the MD simulation, a purely hydrodynamic simulation was conducted with the Eulerian shock-physics code CTH.[32]. This simulation was performed without allowing chemical reaction and with no attempt to model material strength. The shock properties of PETN were described by a Mie-Gruneisen equation of state taken from the CTH database. A two-dimensional rectangular mesh with a cell size of 1 nm was used. A perfectly rigid material was placed at the $x = 0$ boundary and symmetry was used at the y-dimension boundaries. A 20 nm diameter vacuum-filled void was inserted 120 nm from the rigid wall.

As was done with the MD simulation, the PETN was given a particle velocity toward the rigid wall creating a shock wave that propagated from left to right at a velocity of 4.64 km/s. The shock wave collapsed the void with a result similar to that of the MD simulation, shown in Figure 7. A secondary shockwave is formed by the void-collapse and it spreads radially. A hot spot is formed near the location of void-collapse, and a fan of heated material spreads to the right of the original void, resulting from the interaction of the primary and secondary shockwaves. Because this CTH simulation does not allow for heat-conduction, strength, or chemical reactions the similar result suggests that the early time temperature field observed in the MD simulation is governed by hydrodynamics.

The quantitative differences between the two simulations highlight one benefit of using large-scale reactive MD to study shock phenomena in real materials. For example, the MD simulation includes additional heating from chemical energy release, which raises the temperature of the broad thermal field and magnifies the effect of the hot spot as time progresses. In this CTH simulation, the shock induced heating is primarily due to the equation of state in order to illustrate the phenomena of shockwave induced void collapse.

IV. CONCLUSIONS

We created a micron-scale PETN single crystal with a 20 nm cylindrical void and impacted the crystal with an impact velocity of 1.25 km/s. We used molecular dynamics simulation approach with the Reactive Force Field (ReaxFF) as implemented in the LAMMPS MD package. A supported planar shockwave was driven through the crystal and resulted in void collapse, hot spot formation, chemical reaction initiation, and subsequent hot spot

growth. We observed an exponential growth rate of the hot spot and a strong temporal and spatial coupling between hot spot growth and chemical reactions. We also observed an asymmetrical evolution of hot spot growth, which was a result of the interaction between the primary hot spot and a *secondary hot zone*. It was shown that a secondary circular shockwave was formed upon void collapse, and the combination of the primary planar shockwave and the secondary circular shockwave, creating a *double-shocked region*, was responsible for the secondary hot zone. Results from our ReaxFF molecular dynamics simulations agreed qualitatively well with continuum hydrodynamics simulations using the CTH package.

ACKNOWLEDGMENTS

We appreciate fruitful discussions with Cole Yarrington of Sandia National Laboratories. Sandia National Laboratories is a multi-program laboratory managed and operated by Sandia Corporation, a wholly owned subsidiary of Lockheed Martin Corporation, for the U.S. Department of Energy National Nuclear Security Administration under contract DE-AC04-94AL85000.

---

* Corresponding author. Present address: rshan@materialsdesign.com. Materials Design, Inc., 12121 Scripps Summit Dr, San Diego, California 92131

[1] F. Bowden, M. Stone, and G. Tudor, Proc. R. Soc. Lond. A **188**, 329 (1947).

[2] J. Johnson, P. Tang, and C. Forest, J. Appl. Phys. **57**, 4323 (1985).

[3] J. Dear, J. Field, and A. Walton, Nature **332**, 505 (1988).

[4] D. Dlott and M. Fayer, J. Chem. Phys. **92**, 3798 (1990).

[5] S. Walley, J. Field, and M. Greenaway, Mater. Sci. Technol. **22**, 402 (2006).

[6] C. Coffey, Phys. Rev. B **24**, 6984 (1981).

[7] R. Armstrong, C. Coffey, and W. Elban, Acta Metall. **30**, 2111 (1982).

[8] G. Afanasev, V. Bobolev, Y. Kazarova, and Karabano.YF, Combust., Explos. Shock Waves **8**, 241 (1972).

[9] R. Winter and J. Field, Proc. R. Soc. Lond. A **343**, 399 (1975).

[10] Y. Shi and D. W. Brenner, J. Phys. Chem. B **112**, 14898 (2008).

[11] Q. An, S. V. Zybin, W. A. Goddard III, A. Jaramillo-Botero, M. Blanco, and S. N. Luo, Phys. Rev. B **84**, 220101(R) (2011).

[12] T.-R. Shan, R. R. Wixom, and A. P. Thompson, Proc. 15th International Detonation Symposium , 962 (2014).

[13] J. Mintmire, D. Robertson, and C. White, Phys. Rev. B **49**, 14859 (1994).

[14] M. Kuklja and A. Kunz, J. Phys. Chem. B **103**, 8427 (1999).

[15] N. Bourne and J. Field, Proc. R. Soc. Lond. A **455**, 2411 (1999).

[16] K. Nomura, R. K. Kalia, A. Nakano, and P. Vashishta, Appl. Phys. Lett. **91**, 183109 (2007).

[17] Y. Shi and D. W. Brenner, J. Phys. Chem. C **112**, 6263 (2008).

[18] S. D. Herring, T. C. Germann, and N. Gronbech-Jensen, Phys. Rev. B **82** (2010), 10.1103/PhysRevB.82.214108.

[19] T.-R. Shan and A. P. Thompson, Proc. 15th International Detonation Symposium , 878 (2014).

[20] S. Plimpton, J. Comput. Phys **117**, 1 (1995).

[21] H. M. Aktulga, J. C. Fogarty, S. A. Pandit, and A. Y. Grama, Parallel Comput. **38**, 245 (2012).

[22] A. van Duin, S. Dasgupta, F. Lorant, and W. Goddard, J. Phys. Chem. A **105**, 9396 (2001).

[23] K. Chenoweth, A. C. T. van Duin, and I. Goddard, William A., J. Phys. Chem. A **112**, 1040 (2008).

[24] Y. K. Shin, T.-R. Shan, T. Liang, M. J. Noordhoek, S. B. Sinnott, A. C. T. van Duin, and S. R. Phillpot, MRS Bulletin **37**, 504 (2012).

[25] A. Strachan, A. van Duin, D. Chakraborty, S. Dasgupta, and W. Goddard, Phys. Rev. Lett. **91**, 098301 (2003).

[26] A. van Duin, Y. Zeiri, F. Dubnikova, R. Kosloff, and W. Goddard, J. Am. Chem. Soc. **127**, 11053 (2005).

[27] A. C. T. van Duin, S. V. Zybin, K. Chenoweth, L. Zhang, S.-P. Han, A. Strachan, and I. Goddard, William A., AIP Conf. Proc. **845**, 581 (2006).

[28] J. Budzien, A. P. Thompson, and S. V. Zybin, J. Phys. Chem. B **113**, 13142 (2009).

[29] S. V. Zybin, I. Goddard, William A., P. Xu, A. C. T. van Duin, and A. P. Thompson, Appl. Phys. Lett. **96**, 081918 (2010).

[30] T.-R. Shan, R. R. Wixom, A. E. Mattsson, and A. P. Thompson, J. Phys. Chem. B **117**, 928 (2013).

[31] A. V. Bolesta, L. Zheng, D. L. Thompson, and T. D. Sewell, Phys. Rev. B **76** (2007).

[32] J. McGlaun, S. Thompson, and M. Elrick, Int. J. Impact Eng. **10**, 351 (1990).

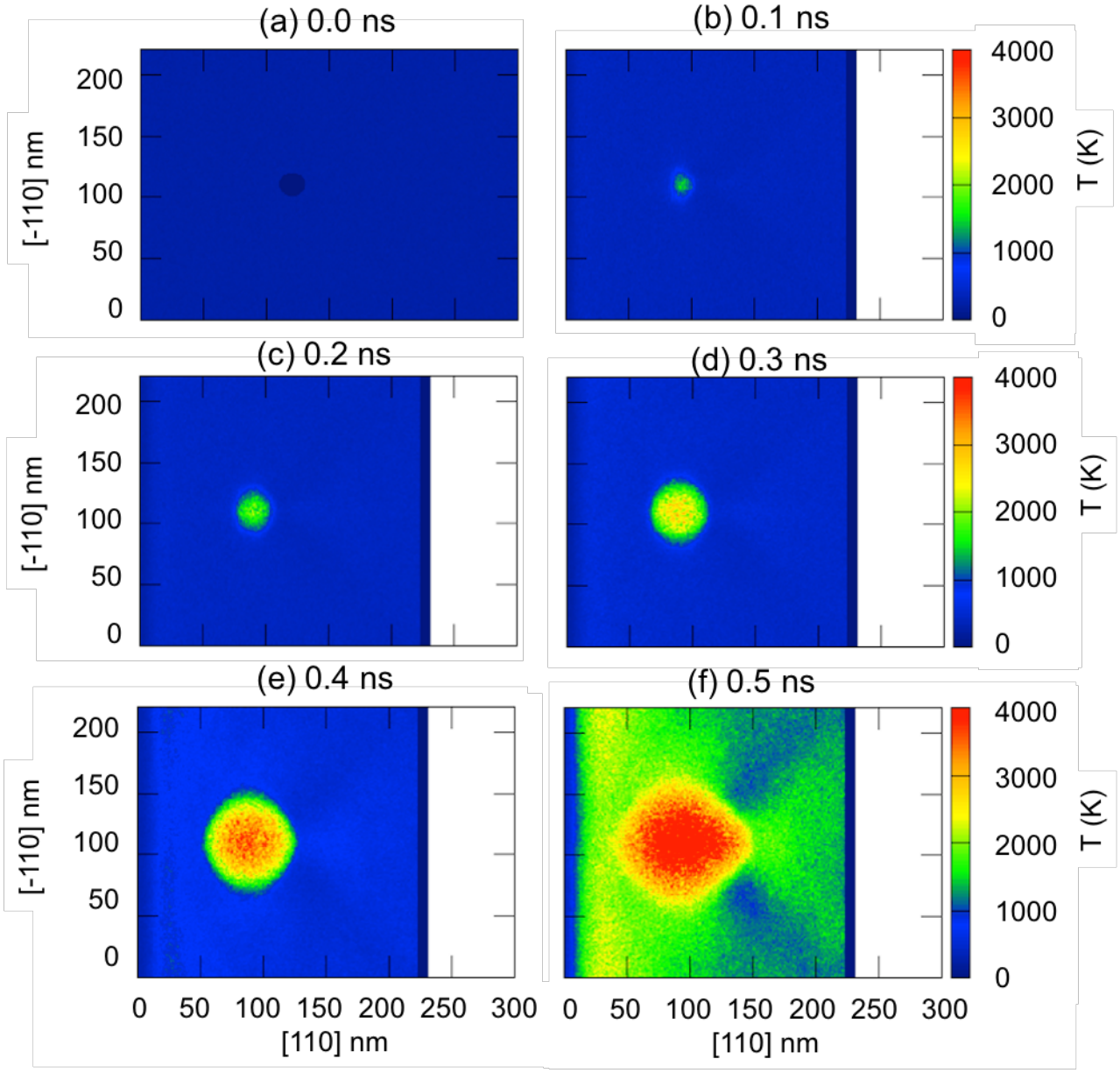

FIG. 1: Sequence of temperature maps from 0 to 0.5 ns illustrating hot spot formation in the PETN crystal containing a 20 nm void. Timing starts after initial impact. Color represents temperature indicated by the color bar. Symmetric hot spot developed after 0.1 ns. Transition to extended asymmetric hot region occurred between 0.4 and 0.5 ns.

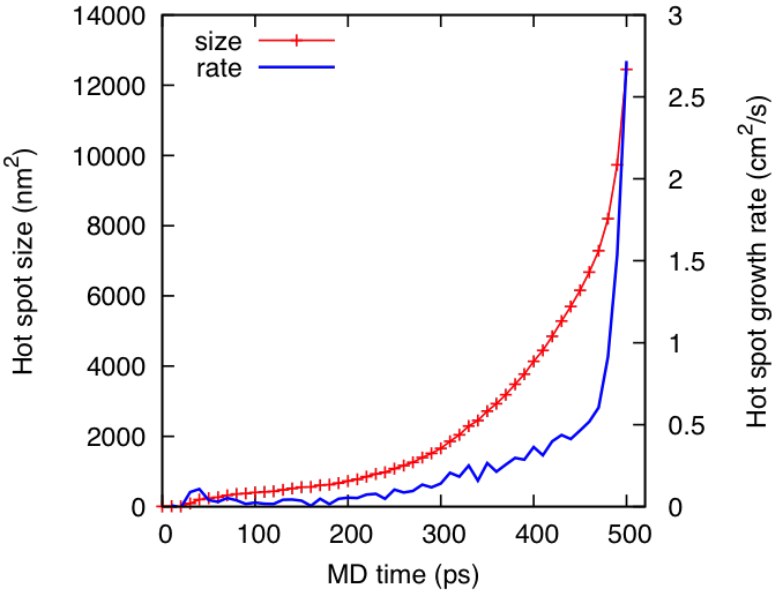

(a)

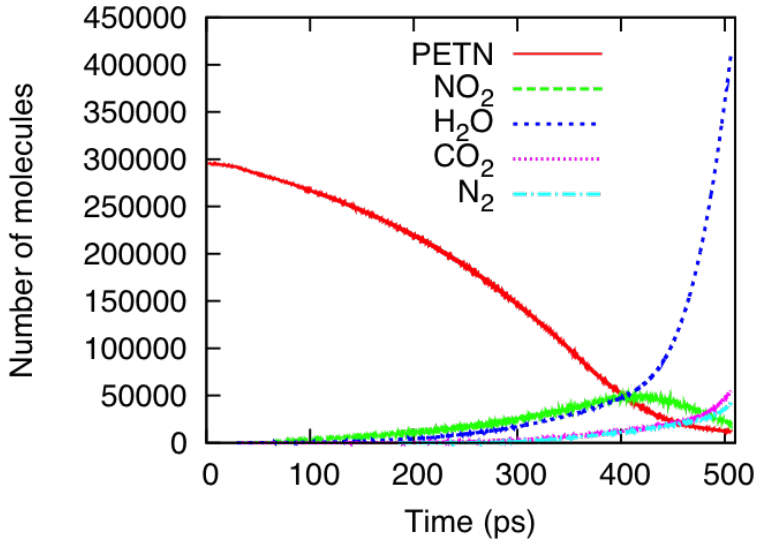

(b)

FIG. 2: Time evolution of (a) hot spot size and growth rate and (b) populations of selected species illustrating a strong coupling between hot spot growth and chemical reactions.

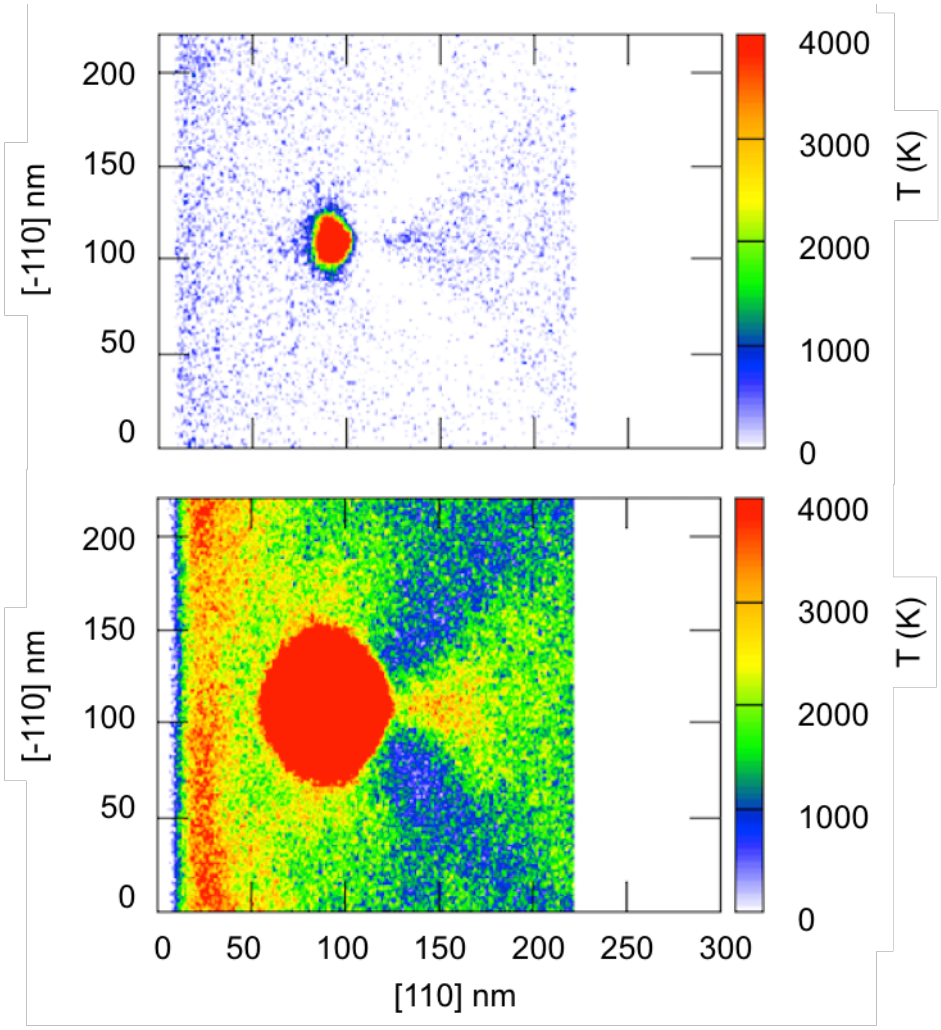

FIG. 3: Temperature maps at (a) 0.1 ns and (b) 0.375 ns after initial impact illustrating the formation of the primary hot spot and the triangular secondary hot zone. Regions with temperature above 800 K (red) and under 400 K (white) are drawn in fixed colors to make the secondary hot zone more discernible.

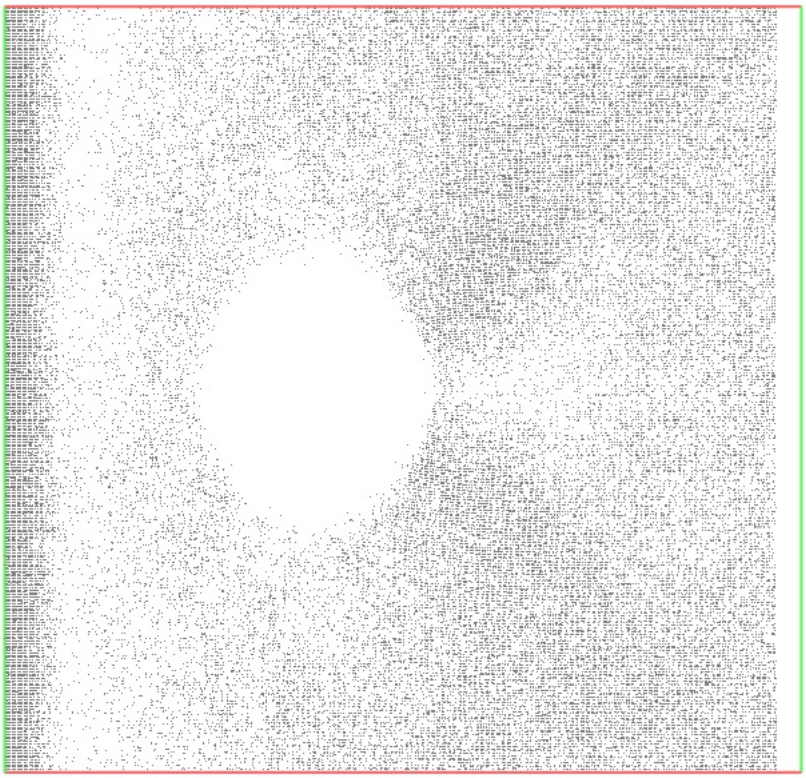

FIG. 4: Distribution of unreacted PETN molecules at 0.375 ns after initial impact, illustrating the primary hot spot and the triangular secondary hot zone.

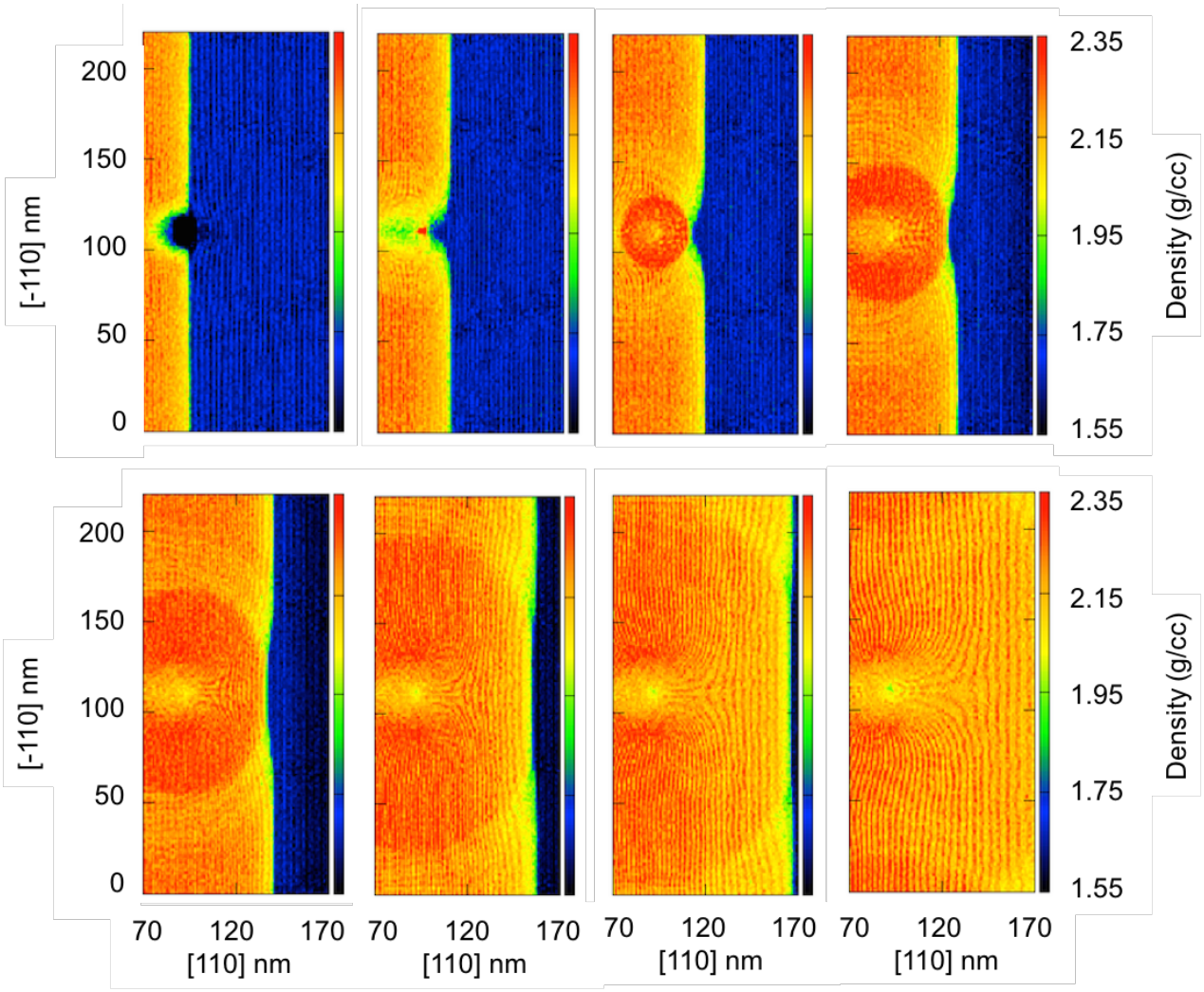

FIG. 5: Sequence of density maps from 25 to 50 ps illustrating the secondary cylindrical shockwave generated by void collapse. Timing starts at initial impact. Void closes at 29 ps, after which the expanding secondary shockwave is discernible.

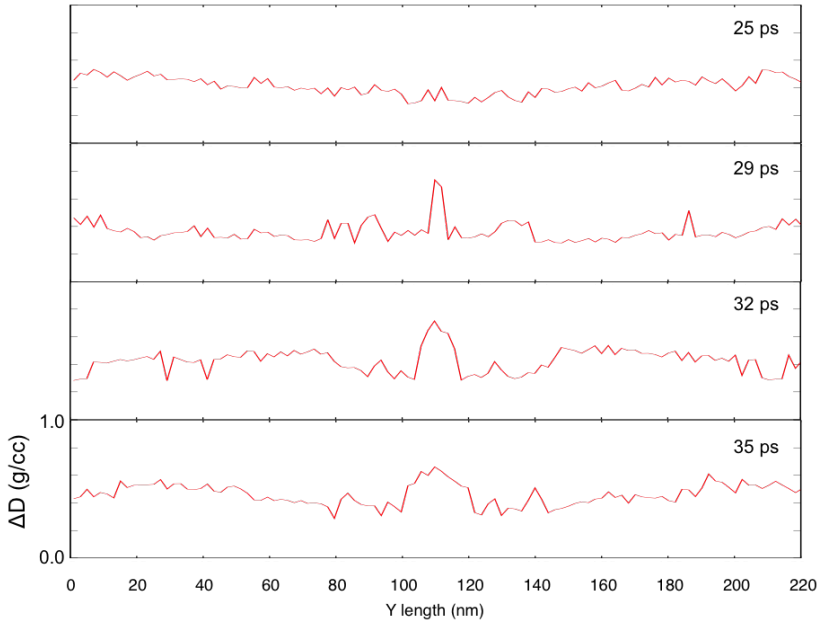

(a) 25-35 ps

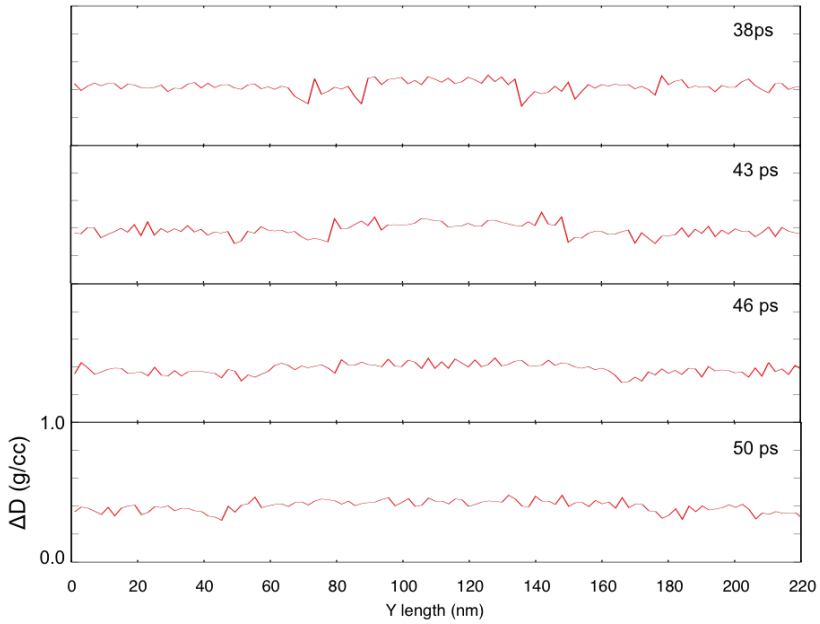

(b) 38-50 ps

FIG. 6: Sequence of density profiles just behind the shock front from 25 to 50 ps illustrating the combined effect of the primary and secondary shockwaves. ΔD indicates the density increase relative to that of the uncompressed material. Distance is measured in the y direction i.e. normal to the shock direction.

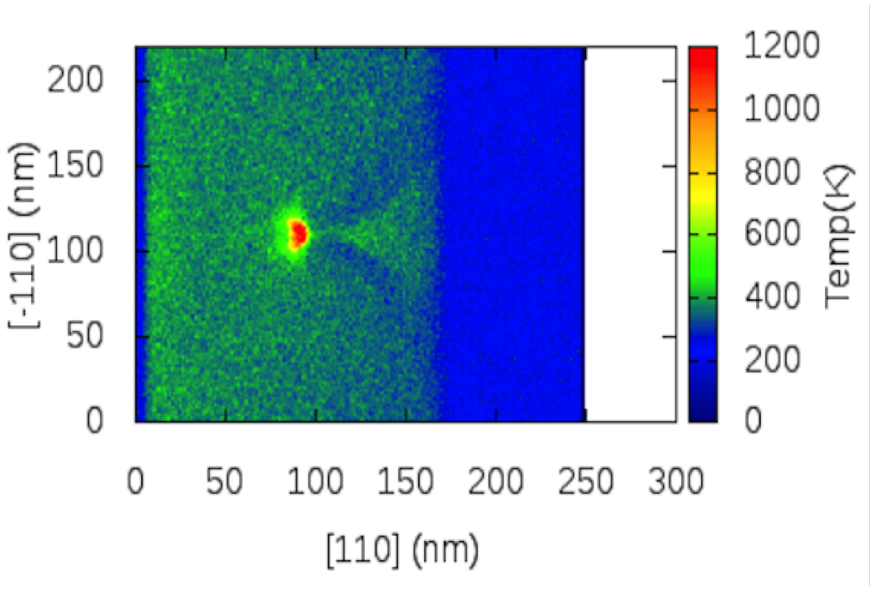

(a) ReaxFF molecular dynamics simulation

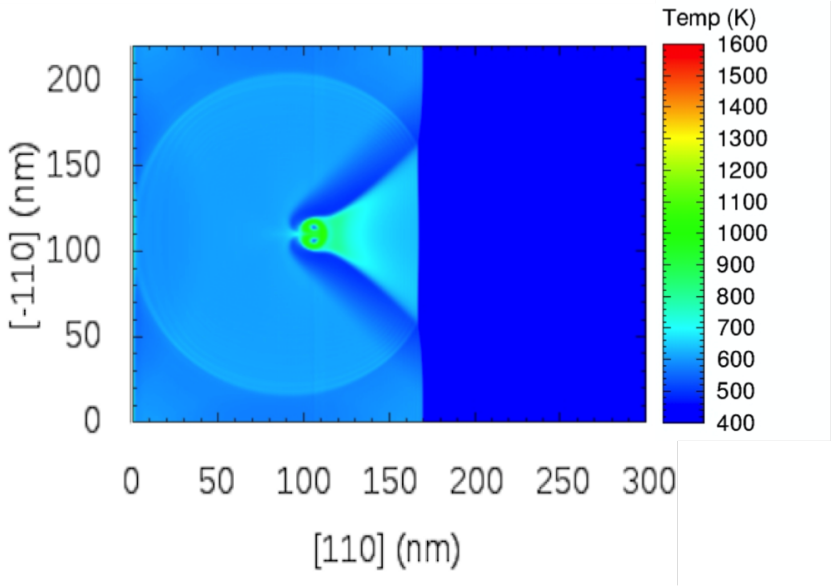

(b) Continuum hydrodynamics simulation

FIG. 7: Temperature maps from (a) ReaxFF molecular dynamics simulation (LAMMPS) and (b) continuum hydrodynamics simulation (CTH) illustrating hot spot formation in the PETN crystal containing a 20 nm void at 48 ps after initial impact. Color represents temperature indicated by the color bar.